catalysts

MDPI

Article

Mesoporous Methyl-Functionalized Titanosilicate Produced by Aerosol Process for the Catalytic Epoxidation of Olefins

Lucia E. Manangon-Perugachi [1,2], Valentin Smeets [1], Alvise Vivian [3], Itika Kainthla [1], Pierre Eloy [1], Carmela Aprile [3], Damien P. Debecker [1] and Eric M. Gaigneaux [1,*]

[1] Institute of Condensed Matter and Nanosciences (IMCN), Université Catholique de Louvain (UCLouvain), Place Louis Pasteur 1, L4.01.09, 1348 Louvain-la-Neuve, Belgium; lucia.manangon@epn.edu.ec (L.E.M.-P.); valentin.smeets@uclouvain.be (V.S.); itika.kainthla@uclouvain.be (I.K.); pierre.eloy@uclouvain.be (P.E.); damien.debecker@uclouvain.be (D.P.D.)

[2] Department of Extractive Metallurgy, Escuela Politécnica Nacional, Quito 170517, Ecuador

[3] Unit of Nanomaterial Chemistry, Department of Chemistry, University of Namur, 5000 Namur, Belgium; alvise.vivian@unamur.be (A.V.); carmela.aprile@unamur.be (C.A.)

* Correspondence: eric.gaigneaux@uclouvain.be

Abstract: Titanosilicates (Ti-SiO_2) are well-known catalysts for the epoxidation of olefins. Isolated Ti inserted in the silica framework in tetrahedral coordination are the active species. Recently, adjusting the hydrophobic/hydrophilic balance of such catalysts' surfaces has appeared as a promising tool to further boost their performance. However, adjusting the hydrophobic/hydrophilic balance via a one-pot classical sol-gel generally leads to a decrease in the Ti dispersion and/or collapse of the pore network. To overcome this limitation, hydrophobic mesoporous Ti-SiO_2 were here synthesized by aerosol-assisted one-pot sol–gel, which allowed the simultaneous control of their Ti loading, degree of methyl-functionalization, and textural properties. Methyl-functionalization was achieved by a partial substitution of tetraethoxy silane (TEOS) by methyltriethoxy silane (MTES) in different ratios. Solid-state ^{29}Si-NMR, FTIR, TGA, and vapor-phase water adsorption showed that methyl moieties were effectively incorporated, conferring a hydrophobic property to the Ti-SiO_2 catalysts. ICP-AES, DRUV, XPS, and N_2 physisorption demonstrated that Ti dispersion and textural properties were both successfully preserved upon the incorporation of the methyl moieties. In the epoxidation of cyclooctene with tert-butyl hydroperoxide as oxidant, the hydrophobic Ti-SiO_2 showed higher catalytic performance than pristine Ti-SiO_2 prepared without MTES. In addition to disentangling the positive effect of adjusting the hydrophobic/hydrophilic balance of epoxidation catalysts on their performance, this contribution highlights the advantages of the aerosol procedure to synthesize mesoporous functionalized catalysts with very high dispersion of active sites.

Keywords: mesoporous titanosilicate TiO_2-SiO_2; aerosol-assisted sol-gel; one-pot methyl-functionalization; surface hydrophobicity; olefin epoxidation

check for updates

Citation: Manangon-Perugachi, L.E.; Smeets, V.; Vivian, A.; Kainthla, I.; Eloy, P.; Aprile, C.; Debecker, D.P.; Gaigneaux, E.M. Mesoporous Methyl-Functionalized Titanosilicate Produced by Aerosol Process for the Catalytic Epoxidation of Olefins. *Catalysts* **2021**, *11*, 196. https://doi.org/10.3390/catal11020196

Academic Editor: Consuelo Alvarez-Galvan

Received: 13 January 2021
Accepted: 27 January 2021
Published: 2 February 2021

Publisher's Note: MDPI stays neutral with regard to jurisdictional claims in published maps and institutional affiliations.

Copyright: © 2021 by the authors. Licensee MDPI, Basel, Switzerland. This article is an open access article distributed under the terms and conditions of the Creative Commons Attribution (CC BY) license (https://creativecommons.org/licenses/by/4.0/).

1. Introduction

To improve heterogeneous catalyst performance, different approaches have been proposed, such as tuning the catalyst texture, controlling the nature and dispersion of the active sites, and optimizing the reaction conditions. Another interesting approach is the adjustment of the hydrophobic/hydrophilic balance of the catalyst surface, which regulates the interaction between the catalyst and the reactants and products and, if well-adjusted, leads to more efficient adsorption of the reactants and desorption of the products. This approach has been proven to enhance catalytic activity, limit side reactions, and improve the stability of diverse catalysts in diverse model reactions [1–8]. Specifically, it was shown that hydrophobic catalysts display better reactivity and stability than their hydrophilic analogs in reactions occurring in the presence of water [9–13].

Olefin epoxidation is important for the fine and bulk chemical industry and allows the study of the effect of adjusting the catalyst hydrophobic/hydrophilic balance. The olefin, which is hydrophobic, reacts with an organic hydroperoxide or hydrogen peroxide to produce the epoxide, which is less hydrophobic. Hence, hydrophobized heterogeneous catalysts should display higher affinity for the olefin and lower affinity for the epoxide. A wide variety of Ti-containing materials, such as TS-1 [14–17], Ti-beta [18,19], Ti-SBA-15 [20–22], Ti-MCM-41 [23–26], Ti/SiO_2 [18,25,27,28], and Ti-SiO_2 [29–34], have been studied as heterogeneous catalysts for the epoxidation of olefins. Ti in tetrahedral coordination inserted as single atoms in the silica framework (FW-Ti) forms strong Lewis acid species and appears as their active sites [15,31,35–40]. The accepted mechanism for the catalytic epoxidation of olefins with heterogeneous Ti-based catalysts is the Eley–Rideal mechanism [40–42], in which the oxidant adsorbs on the Ti active site and forms active intermediate species [40], which react with the olefin to produce the epoxide that then desorbs from the catalyst.

Various attempts have been made to boost the catalytic performance of Ti-containing catalysts [19,29,43–47], but only recently has more attention been paid to the effect of adjusting the hydrophobic/hydrophilic balance and the environment surrounding the active sites on the catalyst surface. Even though the epoxidation mechanism does not require the olefin to adsorb on the catalyst, some affinity is desired so that the olefin can approach the Ti active species on the catalyst surface. It has been indeed shown that hydrophobic Ti-zeolites displayed higher affinity for olefins than hydrophilic ones [48]. Conversely, affinity between the catalyst surface and the epoxide should decrease so that the epoxide desorbs immediately, avoiding undesired consecutive oxidation or ring opening.

In general, two main approaches can be distinguished in the literature to tune the hydrophobicity of Ti-containing catalysts. The first approach is the control of the silanol surface density, which confers a hydrophilic behavior to the catalyst surface, by adjusting the catalyst crystallinity (better crystallized TS-1 have less terminal silanols than Ti-beta and appear more hydrophobic [45]), and by preparing the catalysts in fluoride (F^-) medium (Ti-beta(F) with lower silanol surface density than conventional Ti-beta [49,50]). The high epoxidation activity indeed displayed by these modified catalysts was attributed to their higher hydrophobic character [45,49,50]. The second approach is the functionalization of the catalyst surface with organic moieties by either post-grafting [28,46,51–55] or one-pot functionalization [56–62]. Post-grafting of organosilanes was used to produce hydrophobic Ti-MCM-41 [51], Ti-SBA-15 [51,52]. Ti/SiO_2 [53,54], and Ti-SiO_2 [13]. These hydrophobic catalysts achieved higher yields in the epoxidation of cyclohexene with H_2O_2 or 1-octene with tert-butyl hydroperoxide (TBHP), and some of them even demonstrated higher stability in the presence of water [13,54]. In contrast, hydrophobization by silylation had no significant effect on the epoxidation of 1-hexene and cyclohexene with H_2O_2 catalyzed by either silylated Ti/SiO_2 [28] or silylated TS-1 [46]. Moreover, silylated Ti-beta displayed lower catalytic activity in the epoxidation of 1-hexene with H_2O_2 than the pristine Ti-beta [46]. Markedly, the effect of surface functionalization by post-grafting is different for different Ti-based catalysts. This is explained by the fact that the post-grafting procedure tends to also modify the catalyst structure, texture, and the nature of the active sites.

Direct hydrophobization through one-pot synthesis methods is less time-consuming and can be more efficient than post-modification. Additionally, the functionalization is controlled by the chemistry of the precursors, guaranteeing the functionalization of the desired atoms. Some reports have utilized the one-pot approach to test the effect of adjusting the hydrophobic/hydrophilic balance of Ti-containing catalysts. For example, hydrophobic Ti-SiO_2 and hydrophobic Ti-MCM-41 achieved higher rates and yields in the epoxidation of cyclohexene with tert-butyl hydroperoxide (TBHP) [56–58] and H_2O_2 [58,59]. Contrarily, in other studies, a negative effect of one-pot hydrophobization on the epoxidation of 1-hexene and cyclohexene with TBHP [60,61] was found due to lower surface area, diminished Ti dispersion, and excessive surface functionalization. In addition, one-pot methyl-functionalized Ti-SiO_2 catalysts exhibited similar catalytic performance as their

hydrophilic analogs in the epoxidation of cyclohexene in the presence of water [13]. The negligible effect of hydrophobization was attributed to the lower concentration of surface active sites resulting from the one-pot methyl-functionalization [13]. The results obtained by one-pot functionalization are difficult to compare, and not much research has been conducted to evaluate the catalytic performance per active Ti site and per accessible surface area, so more exploration is necessary to clarify the effect of adjusting the hydrophobic/hydrophilic balance on the epoxidation of olefins.

Recently, we showed that one-pot methyl-functionalization was successful at producing hydrophobic Ti-SiO_2 catalysts that yielded higher epoxidation rates than pristine ones in the epoxidation of cyclooctene, proving the concept that adjusting the hydrophobicity of Ti-SiO_2 catalysts by methyl-functionalization increases their catalytic activity [62]. However, the addition of the methylated precursor disturbed the Ti dispersion and diminished the amount of active sites in the catalyst. This was clearly observed for the catalyst with the highest methyl content, which exhibited the lowest number of active sites compared to the other methyl-functionalized catalysts. Hence, there is a limitation to the degree of methyl-functionalization that can be achieved by this method. Additionally, the specific surface area of the samples was strongly influenced by the degree of methyl-functionalization, which added another variable to be accounted for when comparing the catalysts' performance. These co-dependent variables make the elucidation of functionalization effects challenging; thus, there is a demand for innovative synthesis procedures that allow the control of Ti dispersion, textural properties, and surface functionalization simultaneously.

A method that has been demonstrated to produce catalysts with tailored texture and well-dispersed active species is aerosol-assisted sol-gel (AASG), which is emerging as a practical method to synthesize tailor-made mesoporous catalysts [29,63–69]. The high dispersion of Ti active sites is achieved thanks to the fast drying of the atomized precursor mixture, which quenches the condensation kinetics and leads to the synthesis of materials with homogeneous composition [63]. Moreover, a large variety of templates can be used so as to finely tune the textural properties. In a previous study, we demonstrated that mesoporous Ti-SiO_2 catalysts prepared by AASG are highly effective for the epoxidation of bulky olefins in organic conditions [29].

In this work, we therefore leverage the AASG process to synthesize methyl-functionalized Ti-SiO_2 catalysts. We envisage that the high Ti dispersion achievable with the aerosol method will promote the formation of more active Ti species. In this sense, we hypothesize that methyl-functionalized Ti-SiO_2 catalysts synthesized by AASG will exhibit superior Ti and methyl dispersion as well as higher mesoporosity than previous analogous catalysts synthesized by conventional sol-gel approaches. Such aerosol-synthesized materials are good model materials to study the effect of adjusting the hydrophobic/hydrophilic balance achieved by one-pot surface functionalization on the catalytic epoxidation of cyclooctene with tert-butyl hydroperoxide as oxidant since the textural properties can be kept constant. Furthermore, it is possible to isolate the effect of the hydrophobic/hydrophilic balance thanks to an extended characterization of the catalyst that allows the normalization of the catalytic activity per specific surface area and per Ti active sites.

2. Results and Discussion

2.1. Assessing the Degree of Methyl-Functionalization and Hydrophobicity

Quantitative solid-state ^{29}Si magic-angle spinning (MAS) NMR spectroscopy was used to examine the degree of methyl-functionalization (%Me) of Ti-SiO_2 catalysts (Figure 1). In the ^{29}Si direct excitation (DE) MAS spectra of all Ti-SiO_2 samples, a broad band, assigned to Q^n contributions typical of an amorphous silica matrix, was observed. A deconvolution analysis using Gaussian functions allows the different contributions to be assigned, centered at −112, −102, and −92 ppm, which are attributed to Q^4 ($Si(OSi)_4$), Q^3 ($Si(OSi)_3OH$), and Q^2 ($Si(OSi)_2(OH)_2$) species, respectively. In methyl-functionalized Ti-SiO_2 samples, an additional broad signal centered at −60 ppm revealed the presence of T^3 ($Si(OSi)_3Me$) and T^2 ($Si(OSi)_2(OH)Me$) contributions (deconvolution analysis shown in Figure S1). After

calcination at 623 K, Ti-SiO_2 samples exhibited three degrees of methyl-functionalization—3%, 9%, and 14%—determined from direct excitation NMR experiments by the following formula: $\%Me = 100 \cdot \left(\frac{T^i}{\sum_i (Q^i + T^i)}\right)$. Previous studies have reported that methyl groups strongly bonded to Si were largely preserved upon calcination temperatures as high as 773 K [60–62], which is in agreement with our own observations. Hereafter, our samples will be named TS_Aer-x%Me, where "x" represents the effective percentage of methyl-functionalization found via quantitative solid-state NMR.

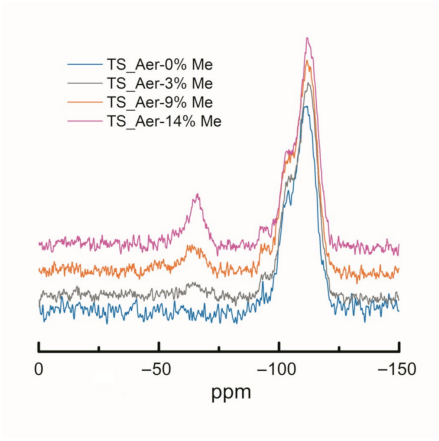


Figure 1. Solid-state ^{29}Si direct excitation MAS-NMR spectra of calcined TS_Aer-x%Me. Spectra are normalized to the Q^4 contribution and are vertically offset for clarity.

Furthermore, FTIR-ATR spectra of the methyl-functionalized samples confirmed the presence of methyl moieties bonded to silicon (υ(Si–C)) at 1279 cm^{-1}, whereas this band was absent in the pristine sample (Figure 2). Qualitatively, the IR spectra of the methyl-functionalized samples follow the same trend as observed by ^{29}Si NMR, with the υ(Si–C) band intensity increasing when increasing the MTES/TEOS ratio in the precursor solution.

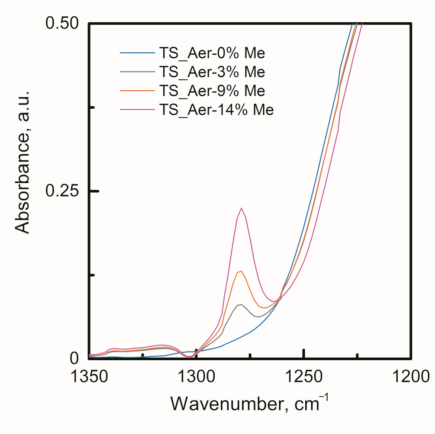


Figure 2. FTIR-ATR spectra of the TS_Aer-x%Me catalysts.

TGA analyses of the pristine catalyst, namely TS_Aer-0%Me (produced only with TEOS as Si precursor), and methyl-functionalized catalysts (TS_Aer-3%Me, TS_Aer-9%Me, TS_Aer-14%Me) were performed to: (i) further verify the presence of methyl moieties, (ii) evaluate the removal of residual templating agents, and (iii) assess the hydrophobic properties by quantification of the physisorbed water (water desorbing in the low temperature range). Three main mass losses were observed in the ranges of 313–453, 453–773, and 773–873 K (Figure 3). The first mass loss was associated with physisorbed water whereas the second mass loss was present equally in the four samples and it was presumably related

to small amounts of organic contaminants, frequently found in such sol-gel samples, that were still present after the calcination (e.g., traces of precursors, solvents, and templating agents). In this work, a mild calcination temperature of 623 K was selected to remove the templating agents while preserving the methyl-functionalization. Lower and higher calcination temperatures, 523 and 723 K, were also tested but the best compromise between templating agent removal and methyl content preservation was found at 623 K. More details about the selection of the calcination temperature can be found in the Supplementary Materials. Interestingly, the third mass loss was only observed in the methyl-functionalized samples. From the derivative curves in Figure 3, this mass loss occurred around 803 K and presented a direct correlation with the degree of methyl-functionalization, thereby suggesting a correspondence with the degradation of the methyl groups, as previously reported in the literature [60–62].

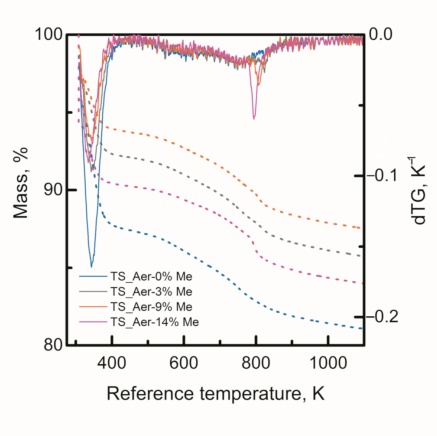


Figure 3. TGA analysis profiles (dotted lines) and derivative curves (solid lines) obtained under air flow for the TS_Aer-x%Me catalysts.

The water desorbed in the 313–453 K range was quantified to assess the degree of hydrophobicity. The derivative curves in Figure 3 suggest that the pristine sample TS_Aer-0%Me desorbed a higher amount of water compared to the methyl-functionalized samples. Nevertheless, a valid comparison of physisorbed H_2O among the samples must be performed after proper normalization to the specific surface area.

N_2 physisorption analyses were performed to properly address the degree of hydrophobicity as well as to understand the effect of the methyl precursor addition on the texture of the catalysts. The N_2 adsorption–desorption isotherms of all samples featured a Type IV isotherm typically associated with mesoporous materials (Figure 4) [70–72]. The specific surface area, excluding the surface area of micropores, was quantified following the strategy described in the Experimental section. T-plots are shown in Figure S3. As shown in Table 1, the samples with a higher degree of methyl-functionalization exhibited higher specific surface areas and lower micropore volumes. All samples had the same pore volume, close to 1.0 cm^3g^{-1}, related to the templating effect of the surfactant (Table 1). The pore size distributions (PSD) determined from the BJH method did not vary significantly despite the addition of the methyl precursor, as the mesopore distribution remained centered at ca. 12 nm (Figure 4, inset). These results demonstrate that, unlike Ti-SiO_2 prepared by conventional sol-gel techniques [13,60,61], the catalysts prepared by aerosol-assisted sol-gel show no alteration of their mesostructure upon the incorporation of methyl groups during the synthesis. Additionally, SEM images of TS_Aer-0%Me and TS_Aer-9%Me, given in the Supplementary Materials (Figure S4), showed that pristine and methyl-functionalized catalysts are formed of microspheres with similar size in the range of 1 to 20 μm.

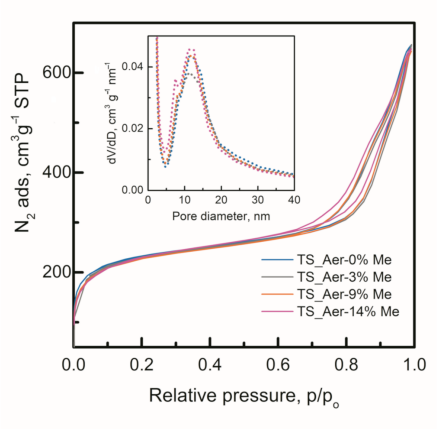


Figure 4. N_2 physisorption isotherms of TS-Aer x%Me catalysts. Pore size distributions (PSDs) based on the desorption branch of the isotherms are shown in inset.

Table 1. Textural properties of the TS_Aer x%Me catalysts.

Sample	$SSA_{corrected}$ [a] $m^2\ g^{-1}$	Pore volume (77 K) [b] $cm^3\ g^{-1}$	Micropore volume (77 K) [c] $cm^3\ g^{-1}$
TS_Aer-0%Me	360	1.00	0.21
TS_Aer-3%Me	364	1.00	0.20
TS_Aer-9%Me	402	0.98	0.18
TS_Aer-14%Me	462	0.99	0.16

[a] Specific surface area corrected by excluding the N_2 uptake due to micropore filling. [b] N_2 volume taken up at 77 K and relative pressure of 0.99. [c] Determined from the intercept of the best tangent drawn in the t-plot in the relative pressure range of 0.05–0.30.

The degree of hydrophobicity was then assessed by three different approaches (Table 2). First, the amount of physisorbed water (calculated from TGA data) was normalized by the specific surface area $SSA_{corrected}$ to eliminate the difference in surface area. As expected, the pristine sample TS_Aer-0%Me presented the highest content of physisorbed water, whereas the methyl-functionalized samples displayed smaller amounts of physisorbed water per unit of surface area (Table 2). In general, methyl-functionalized catalysts exhibited a stronger hydrophobic character than the pristine one. However, this approach did not allow proper correlation of the methyl content with the degree of hydrophobicity since all methyl-functionalized catalysts displayed similar amounts of physisorbed water. Therefore, in a second approach, the fraction of Si atoms coordinated to –OH groups (hydrophilic sites) was estimated from the contributions of Q^3 and Q^2 species in ^{29}Si solid-state MAS NMR spectra (that correspond to the Si atoms existing as $(OSi)_3SiOH$ and $(OSi)_2Si(OH)_2$. This strategy has been used previously to assess the degree of hydrophobicity of a material based on the quantification of the fraction of Si atoms existing as distinct silanol species [49,73]. As shown in Table 2, this analysis showed that the fraction of Si as $(OSi)_3SiOH$ and $(OSi)_2Si(OH)_2$ decreased with increasing amount of methyl content. Third, in order to allow a better comparison of the hydrophilic/hydrophobic character of the catalysts, water vapor sorption experiments were performed at 295 K. Figure 5 shows the vapor water adsorption isotherms normalized to the specific surface area ($SSA_{corrected}$) at low relative pressures. The affinity of the catalyst surface for water is featured at low relative pressures of the adsorption branch of the isotherm [74,75]. The adsorption isotherms in the whole relative pressure range are shown in Figure S4. The normalized water uptake at selected relative pressures of $p/p_o = 0.1$ and 0.2 is displayed in Table 2. A reduced affinity for water was featured by TS_Aer-9%Me and TS_Aer-14%Me compared to the pristine TS_Aer-0%Me, thus confirming the results from TGA analysis. Interestingly, the water sorption isotherms revealed that the TS_Aer-14%Me catalyst was more hydrophobic than the TS_Aer-9%Me catalyst, regarding its lower H_2O uptake, which is in agreement with its

methyl content. Notably, at relative pressures lower than 0.15, a difference in hydrophobicity between TS_Aer-0%Me and TS_Aer-9%Me is not marked due to the normalization to $SSA_{corrected}$, which has an associated uncertainty in the measurement of 5% and does not account for micropores filled at low relative pressures. The difference in hydrophobicity becomes clearer at relative pressures higher than 0.15.

Table 2. Physisorbed water per specific surface area, fraction of Si atoms existing as Q^3 ($Si(OSi)_3OH$) or Q^2 ($Si(OSi)_2(OH)_2$), and water uptake at $p/p_o = 0.1$ and $p/p_o = 0.2$ for TS_Aer-x%Me.

Sample	Phys $H_2O/SSA_{corrected}$ [a] $mol_{H2O}\ m^{-2}$	Fraction of Si as Q^3 and Q^2 species [b] mole %	H_2O Uptake at p/po = 0.1 [c], $mol_{H2O}\ m^{-2}$	H_2O Uptake at p/po = 0.2 [c], $mol_{H2O}\ m^{-2}$
TS_Aer-0%Me	22.3	32.1	5.1	11.6
TS_Aer-3%Me	13.2	31.5	n.m. [d]	n.m. [d]
TS_Aer-9%Me	9.3	30.7	5.1	9.1
TS_Aer-14%Me	13.1	24.2	3.4	6.1

[a] Determined from the TGA analysis and the specific surface area corrected ($SSA_{corrected}$) given in Table 1. [b] Determined from ^{29}Si solid-state direct excitation MAS NMR by the formula: $\%SiOH = 100 \cdot \left(\frac{Q^3 + Q^2}{\sum_i (Q^i + T^i)}\right)$ (Figure 1). [c] Determined from the vapor water sorption analysis. [d] Not measured.

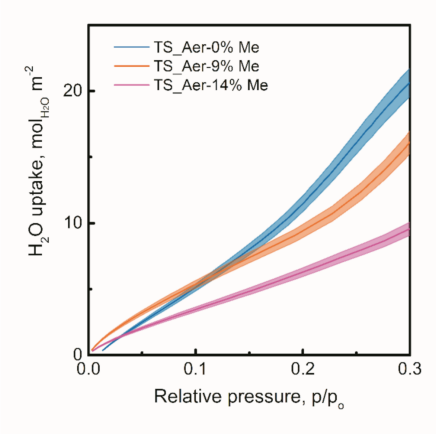


Figure 5. Vapor water adsorption isotherms normalized by the specific surface area ($SSA_{corrected}$) at low relative pressures. The normalized water uptake values are depicted on the curve and the shaded regions denote the estimated uncertainty of 5% due to the N_2 physisorption measurement of $SSA_{corrected}$.

In summary, one can infer from the characterization presented above that (i) our aerosol protocol was successful at incorporating methyl moieties in the samples, in particular that a large proportion of the methyl moieties survived the thermal treatment applied after synthesis, (ii) all aerosol-made samples exhibit a very similar mesoporous texture featuring more accessible surfaces for the epoxidation reaction than the ones obtained by conventional sol-gel, and (iii) the methyl-functionalized samples are more hydrophobic than the pristine one.

2.2. Quantification of Ti Dispersion

Diffuse reflectance UV-Vis (DRUV) spectroscopy was performed to distinguish framework Ti (FW-Ti) in the range 200-240 nm from extra-framework Ti (EFW-Ti) in the range of 240-330 nm [38,76–78]. While FW-Ti corresponds to Ti atoms in tetrahedral coordination, EFW-Ti corresponds to Ti atoms in higher coordination numbers such as pentahedral or octahedral coordination [38,76,79]. The latter species are the same Ti species found in anatase (crystalline TiO_2), and their presence can be detected by DRUVS in the range 310–330 nm [38,76,77]. Pristine and methyl-functionalized catalysts exhibit both FW-Ti and EFW-Ti species (Figure 6). The contribution of FW-Ti species is significantly higher than

that of EFW-Ti, and no contribution above 310 nm was detected, excluding the formation of TiO_2 nanodomains. This is evidence of the high Ti dispersion that was achieved by the aerosol synthesis method. The samples TS_Aer-9% Me and TS_Aer-14% Me exhibit slightly higher amounts of EFW-Ti than the TS_Aer-3% Me and this should be kept in mind when discussing their catalytic activity.

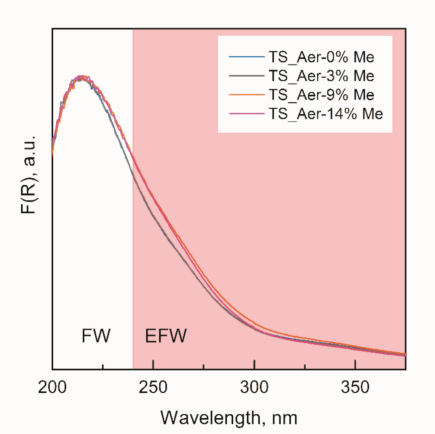


Figure 6. DRUV spectra of the TS_Aer-x%Me catalysts. The white region corresponds to the FW-Ti species and the red region corresponds to the EFW-Ti species.

The difference in Ti dispersion among the samples was quantified by calculating the band gap energy values (Eg) for each sample. The Eg value has been used in several studies to follow the evolution of the structure/coordination of titanium at different loadings [18,80]. In this study, Eg was calculated from the optical absorption edge in the DRUV spectra using the Tauc method and considering a direct allowed transition [81]. The calculated Eg was plotted as a function of the methyl-functionalization degree (Figure 7). The calculation of the Eg value for each sample is shown in the Supplementary Materials (Figure S6).

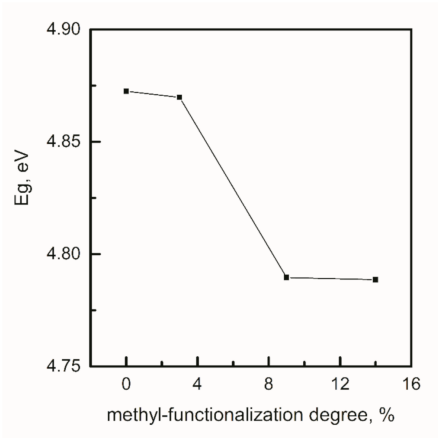


Figure 7. Influence of the methyl-functionalization degree on the band gap energy values (Eg) for TS_Aer-x%Me catalysts.

Higher Eg values are due to the presence of tetrahedral Ti (FW-Ti) corresponding to a higher Ti dispersion, whereas poorly dispersed species in octahedral coordination spheres (EFW-Ti) generate a lower Eg value. The value calculated for TS_Aer-0%Me fell in the range of the Eg values calculated for other Ti-SiO_2 catalysts synthesized by Smeets et al. [29] and De Clercq et al. [80]. As shown in Figure 7, TS_Aer-0% Me and TS_Aer-3% Me exhibited higher Eg values than TS_Aer-9%Me and TS_Aer-14%Me. This was attributed to the presence of EFW-Ti in the samples with a higher methyl-functionalization

degree. This trend was supported by a previous study, where methyl-functionalization via one-pot synthesis contributed to the formation of EFW-Ti in the catalyst [62]. In the present work, aerosol-assisted sol-gel was applied in the attempt to diminish this detrimental effect on the catalyst homogeneity. After comparing the Eg values range (4.03–4.65 eV) measured for similar pristine and methyl-functionalized Ti-SiO_2 catalysts synthesized by the conventional sol-gel method in a previous work [62] against the Eg values range (4.79–4.87 eV) measured for the aerosol catalysts, it is clear that the aerosol synthesis procedure allowed the preservation of the dispersion of the Ti active sites in the presence of the MTES co-precursor. The calculations of the Eg values for the conventional sol-gel samples can be found in the Supplementary Materials (Figure S7).

To further evaluate the homogeneity and the Ti surface dispersion in the TS_Aer-x%Me catalysts, bulk and surface atomic Ti/(Si+Ti) ratios were determined by Inductively Coupled Plasma-Atomic Emission Spectroscopy (ICP-AES) and X-ray photoelectron spectroscopy (XPS), respectively. Bulk atomic Ti/(Si+Ti) ratios were found to be equal to the nominal Ti/(Ti+Si) molar ratio (0.020) in all samples (Table 3), meaning that the composition of the catalysts is well-controlled in the aerosol process, both in the presence and absence of the methylated precursor. Surface atomic Ti/(Si+Ti) ratios for all catalysts were calculated based on the decomposition of the XPS Ti 2p spectra and the XPS elemental quantification, which is shown in Supplementary Materials, Table S2. The Ti 2p spectrum is composed of two spin-orbit components (Ti $2p_{3/2}$ and Ti $2p_{1/2}$) which are separated by 5.7 eV [82]. While the Ti $2p_{3/2}$ binding energy of pure TiO_2 is 458.5 eV (octahedral coordination) [82,83], it is known that Ti in titanosilicate displays peak broadening and shift to higher binding energy (BE) [29,62,80,84,85]. In fact, the Ti $2p_{3/2}$ peak can be decomposed considering two kinds of Ti species: FW-Ti (460.0 eV) [83,86–88] and EFW-Ti (458.5 eV) [82,83]. As shown in Figure 8, the binding energy values of the Ti doublet of the TS_Aer-x%Me catalysts were shifted to values higher than 458.5 eV and exhibited peak broadening, suggesting the presence of FW-Ti species. Therefore, the Ti 2p peak decomposition of our catalysts was performed, and further details on the peak decomposition are included in the Supplementary Materials. Here, we found that the FW-Ti species fell at the binding energy of 460.0 eV, whereas the EFW-Ti species fell at 458.5 eV, consistent with the literature [29,83,86–89]. As indicated in Table 3, the Ti surface content increased slightly in more methyl-functionalized samples. On the contrary, the atomic fraction of FW-Ti over total Ti on the surface gradually diminished in more methyl-functionalized samples. These results reveal some heterogeneity in the TS_Aer-x%Me catalysts due to the presence of the methyl precursor that caused slight Ti enrichment on the catalyst surface and affected its dispersion. This supports DRUVS observations. Even though small heterogeneities were detected in the aerosol samples, the Ti dispersion was superior to that reached by the conventional sol-gel method (Surf. FW-Ti/Ti of around 0.70) [62]. Additionally, XPS confirms that more methyl-functionalized samples have higher content of C and specifically higher content of the C–(C,H) component per Si atom, which is likely related to the presence of methyl moieties on the catalyst surface. This result is consistent with NMR, FTIR, and TGA characterization of the methyl-functionalization degree in the TS_Aer-x%Me catalysts.

Table 3. Bulk atomic ratios based on ICP-AES and surface atomic ratios based on XPS elemental quantification.

Sample	Bulk Ti/(Si+Ti) at. Ratio	Surf. Ti/(Si+Ti) at. Ratio	Surf. FW-Ti/(Si+Ti) at. Ratio	Surf. FW-Ti/Ti at. Ratio	Surf. C/(Si+Ti) at. Ratio	Surf. C–H/Si at. Ratio
TS_Aer-0%Me	0.020	0.015	0.013	0.85	0.227	0.133
TS_Aer-3%Me	0.020	0.016	0.013	0.83	0.282	0.191
TS_Aer-9%Me	0.020	0.017	0.014	0.79	0.306	0.205
TS_Aer-14%Me	0.020	0.019	0.014	0.77	0.383	0.273

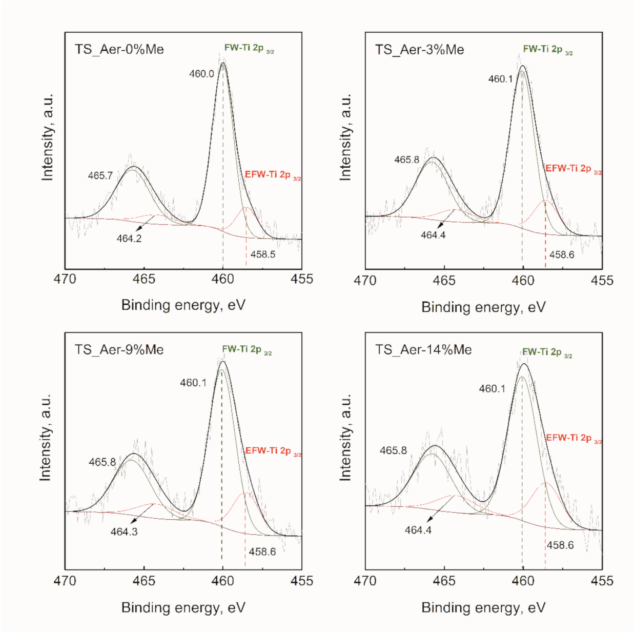


Figure 8. Decomposition of XPS Ti 2p spectra with two components FW-Ti (green solid line) and EFW-Ti (red solid line). The measured spectra are represented by the gray solid line and the corresponding fit is represented by the black solid line (sum of FW-Ti and EFW-Ti components). The BE of FW-Ti 2p $_{3/2}$ is represented by the green dashed line and the BE of EFW-Ti 2p $_{3/2}$ is represented by the red dashed line.

Summarizing, the combination of results from XPS, DRUV, and ICP-AES revealed that one-pot methyl-functionalized samples with identical bulk Ti content (0.020) exhibited higher Ti total content on their surfaces along with a slightly lower proportion of FW-Ti species as compared to the pristine one. Further comparison among the samples is required by determining their respective number of atoms of Ti and FW-Ti per unit of surface area. As depicted in Table 4, all catalysts exhibited similar Ti and FW-Ti surface density, except for the sample TS_Aer-14%Me, which seemed to have a smaller surface density of FW-Ti species as compared to the others.

Table 4. Ti and FW-Ti surface density on the catalysts TS_Aer-x%Me.

Sample	Ti atoms·nm^{-2} *	FW-Ti atoms·nm^{-2} *
TS_Aer-0%Me	0.37	0.32
TS_Aer-3%Me	0.40	0.32
TS_Aer-9%Me	0.37	0.31
TS_Aer-14%Me	0.37	0.27

* An example of the calculation is shown in Supplementary Materials.

2.3. Catalytic Performance of Hydrophobic Mesoporous Ti-SiO_2 on the Epoxidation of Cyclooctene

Pristine and methyl-functionalized mesoporous catalysts were compared in the epoxidation of cyclooctene with tert-butyl hydroperoxide as oxidant. The catalytic activity was assessed by following the epoxide production as a function of the reaction time (Figure 9). The epoxide production was normalized by the specific surface area ($SSA_{corrected}$, see Table 1) to discriminate the detected effect of methyl-functionalization on the catalyst texture. The effect of the pore size was not taken into account as all catalysts displayed similar pore size distributions (see Figure 4, inset).

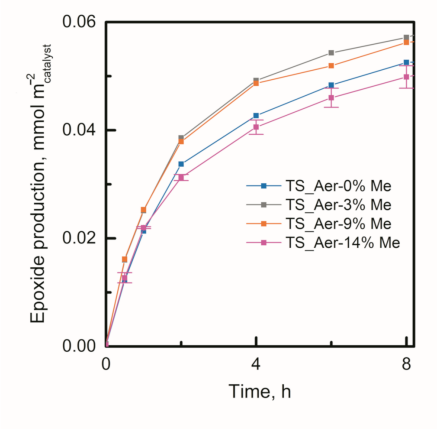


Figure 9. Kinetic data in terms of epoxide production per unit of surface area ($SSA_{corrected}$) for the reaction of cyclooctene with TBHP. Error bars are shown for TS_Aer-14%Me (n = 3).

As shown in Figure 9, hydrophobic catalysts with effective methyl-functionalization of 3% and 9% produced more epoxide per unit of surface area than the pristine catalyst, displaying a positive effect of hydrophobization on the catalytic activity. This is in agreement with our initial hypothesis that the high affinity of a hydrophobized catalyst for the olefin facilitates the olefin approaching to the active epoxidation sites on the catalyst surface. However, the methyl-functionalized sample with 14% as effective methyl content showed lower performance.

The carbon balance was close to 100% for all the experiments and no other product than the epoxide was detected, so the selectivity was 100% towards the epoxide. TBHP conversions measured during reaction experiments are shown in the Supplementary Materials (Figure S8).

Further discussion of the effect of hydrophobicity on the catalytic activity requires consideration of the Ti surface density since the catalyst characterization indicated that methyl-functionalization affects not only the surface polarity but also the number of the Ti atoms present at the surface. The pristine catalyst TS_Aer-0%Me contained as many FW-Ti species per unit of surface area as TS_Aer-3%Me and TS_Aer-9%Me, so their epoxide production should be similar if assumed on the basis of this criterion only. Inversely, TS_Aer-3%Me and TS_Aer-9%Me produced more epoxide per unit of surface area as compared to TS_Aer-0%Me, confirming the positive effect of methyl-functionalization. The loss of performance for TS_Aer-14%Me, unlike the tendency observed for TS_Aer-3%Me and TS_Aer-9%Me, could be explained by its lower content of active FW-Ti species available at the surface. Indeed, after normalization to the number of FW-Ti species (Figure 10), the epoxide production of TS_Aer-14%Me reached that of TS_Aer-3%Me and TS_Aer-9%Me. An excessive methyl-functionalization degree induces a lower content of FW-Ti that diminishes the catalytic activity. Notably, all methyl-functionalized samples displayed better catalytic activity than TS_Aer-0%Me. This was also verified in terms of TOF for TBHP conversion at the initial stage of the reaction (30 min) over TS_Aer-x%Me. Estimated TOF values were 44, 45, and 57 h^{-1} over TS_Aer-3%Me, TS_Aer-9%Me, and TS_Aer-14%Me, respectively. TOF over methyl-functionalized catalysts was higher than that over TS_Aer-0%Me (38 h^{-1}). An example of TOF calculation is shown in the Supplementary Materials. These results prove that methyl-functionalization and its corresponding hydrophobicity improved the catalytic performance in the epoxidation of cyclooctene.

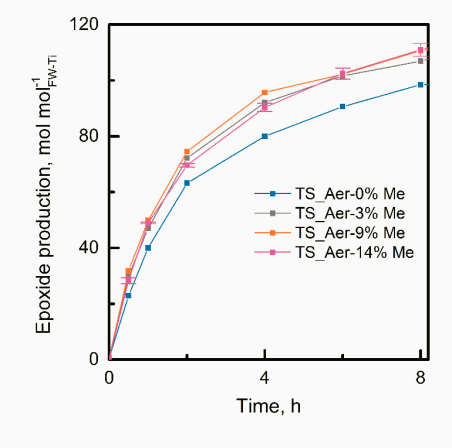


Figure 10. Epoxide production normalized by the number of FW-Ti species on the surface of the TS_Aer-x%Me catalysts. Error bars are shown for TS_Aer-14%Me.

3. Materials and Methods

3.1. Preparation of Methyl-Functionalized Mesoporous Titanosilicate via Aerosol-Assisted Sol-Gel

The catalysts were prepared via one-pot aerosol-assisted sol-gel to achieve good Ti and methyl dispersion as well as good textural properties. A fraction of tetraethoxy silane precursor (TEOS, Sigma-Aldrich, Diegem, Belgium, 98%) was substituted by a more hydrophobic alkyl silane, namely methyltriethoxy silane (MTES, Sigma-Aldrich, Diegem, Belgium, 99%), to obtain hydrophobic methyl-functionalized mesoporous catalysts with Ti incorporated by the addition of titanium butoxide (TiBut, Sigma-Aldrich, Diegem, Belgium, 97% reagent grade) in Ti/(Si+Ti) molar ratio equal to 0.02 in all samples.

The procedure for the catalyst synthesis was adapted from Smeets et al. [29]. Precisely, the precursor solution was prepared by adding 0.6 mmol TiBut dropwise to 79 mmol tetrapropyl ammonium hydroxide (TPAOH, Merck, Darmstadt, Germany, 40%). After 10 min stirring, 513.6 mmol distilled water was poured and stirred for an additional 10 min. Then, 29.4 mmol TEOS and MTES were successively added and the final mixture was stirred overnight at room temperature in a closed vessel to hydrolyze the precursors. Afterwards, the solution was aged in the oven at 343 K for 15 h. Then, 0.2 mmol Pluronic F127 (F127, BASF, Ludwigshafen, Germany) was added and the solution was stirred for 1 h prior to atomization. The final molar composition of the precursor solution was x MTES: 1 − x (TEOS + TiBut): 0.15 TPAOH: 0.005 F127: 19.6 H_2O, where "x" represents the molar fraction of MTES used in the synthesis of the hydrophobic samples, as defined in Equation (1). In the case of the pristine sample, no MTES was added to the mixture (i.e., x = 0). For the methyl-functionalized samples, the MTES molar ratios used were 0.05, 0.10, and 0.20, as defined in Equation (1).

$$Molar\ ratio_{MTES} = \frac{mol_{MTES}}{mol_{TEOS} + mol_{TiBut} + mol_{MTES}} \quad (1)$$

The clear precursor solution was sprayed by a Büchi Mini Spray Drier B-290 (Büchi Labortechnik AG, Flawil, Switzerland) with a liquid flow rate of 5 mL/min and an air pressure of 4 bars. The atomized sol was dried by traveling through a glass reactor fed with air heated at 493 K. Under these conditions, the exit gas had a temperature of 393 K. The powder was collected and aged at 343 K overnight in a static oven. After aging, the powder was calcined in static air along a temperature program that started with a ramp of 1 K min^{-1} from room temperature to 623 K and followed by a dwell step at the final temperature for 10 h. After cooling down inside the furnace for around 3 h, the calcined solids were stored in a desiccator.

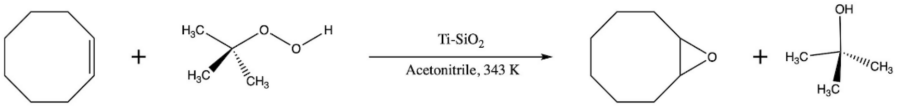
3.2. Catalyst Characterization

Solid-state ^{29}Si direct excitation magic-angle spinning nuclear magnetic resonance (^{29}Si-DE-MAS-NMR) spectra were recorded on a Bruker Avance-500 (Bruker, Brussels, Belgium) spectrometer operating at 11.7 T (99.3 MHz for ^{29}Si) and equipped with a 4 mm cross polarization magic-angle spinning (CP-MAS) Bruker probe under ambient conditions. The sample was loaded into a 4 mm zirconia rotor (around 100 mg) and measured with a spinning frequency of 8 kHz. The acquisition parameters were 300 s relaxation delay, 3 µs (90°) excitation pulse, 52 ms acquisition time. The processing consisted of exponential multiplication of the free induction decay (FID) with a line broadening factor (lb) of 30 Hz, zero-filling, Fourier transform, phase and baseline corrections performed on the Bruker TopSpin v2.1 software. Chemical shifts were referenced with respect to tetramethylsilane (fixed at 0 ppm). Fourier transform infrared (FTIR) measurements were performed in attenuated reflectance mode (ATR) using an IFS55 Equinox Bruker spectrometer (Bruker, Brussels, Belgium) equipped with a DTGS detector. The spectra were obtained by recording 100 scans in the range from 400 to 4000 cm^{-1} at a resolution of 4 cm^{-1}. The spectra were analyzed using the software OPUS. Thermal gravimetric analysis (TGA) was performed on a TGA/DSC 3^+ STAR System (Mettler Toledo, Zaventem, Belgium). A typical method was a ramp from 303 to 1173 K at 10 K min^{-1} under air flow (50 mL min^{-1}, 80% N_2 and 20% O_2, Alphagaz Air Liquide, Brussels, Belgium). Diffuse reflectance UV-Vis (DRUV) spectra were recorded on a Shimadzu UV-Vis-NIR spectrometer (Shimadzu Benelux, The Netherlands) equipped with a Praying Mantis in a spectral range from 200 to 600 nm using the Shimadzu UV software package. A Spectralon pellet was used to measure the background spectrum, and the Kubelka–Munk function F(R) was calculated based on the reflectance (R). The band gap energy value (Eg) was calculated from the optical absorption edge in the DRUV spectra using the Tauc method. To verify the effective Ti content, the Ti-SiO_2 samples were analyzed by inductively coupled plasma–atomic emission spectroscopy (ICP-AES) on an ICAP 6500 instrument (Thermo Fisher Scientific Inc., Waltham, MA, USA). The samples were calcined at 823 K for 24 h to remove the organic matter and then were decomposed by sodium peroxide fusion in carbon crucibles. X-ray photoelectron spectroscopy (XPS) experiments were performed on a SSX-100/206 photoelectron spectrometer (Surface Science Instruments, USA) equipped with a monochromatized micro focused Al X-ray source (powered at 10 kV and 20 mA), a 30° solid angle acceptance lens, a hemispherical analyzer, and a channel plate detector. Samples were pressed into clean stainless-steel troughs of 6-mm diameter and placed on a ceramic carousel. Samples were degassed inside the sample introduction chamber overnight and transferred to the analysis chamber, where pressure was around 10^{-6} Pa. The angle between the surface normal and the axis of the analyzer lens was 55°. The area of analysis was approximately 1.4 mm^2 and the passing energy was set at 50 eV. Under these conditions, the full width at half maximum (FWHM) of the Au 4f 7/2 peak of a clean gold standard sample was around 1.1 eV. Charging effects were stabilized using a flood gun set at 8 eV and a fine-meshed Ni grid placed 1 mm above the sample surface. The following sequence of spectra was recorded: survey spectrum, C 1s, O 1s, Ti 2p, Si 2p, and C 1s again to check the stability of charge compensation with time and the absence of sample degradation. The binding energy scale was referenced to the C–(C,H) component of the C 1s peak of carbon fixed at 284.8 eV. Peak decomposition was performed with the CasaXPS processing software (Casa Software Ltd., Teignmouth, UK). C 1s and Ti 2p spectra were decomposed with the least squares fitting routine provided by the software with a Gaussian/Lorentzian (85/15) product function and after subtraction of a non-linear Shirley baseline. Surface elemental composition was calculated using peak areas normalized on the basis of acquisition parameters and sensitivity factors provided by the manufacturer. N_2 adsorption–desorption experiments were performed at 77 K using a Micromeritics Tristar 3000 (Micromeritics, Brussels, Belgium). Before the analysis, the samples were degassed overnight under vacuum (6.7 Pa) at 453 K. Adsorption–desorption isotherms were obtained and the micropore volume was determined from the t-plot constructed based on the adsorption data. The intercept of the best tangent drawn on the t-plot in the

range corresponding to partial pressures between 0.05 and 0.30 of the t-plot was used to determine the micropore volume, which was then subtracted from the N_2 volume adsorbed at each data point to construct a second adsorption isotherm. The Brunauer-Emmet-Teller (BET) method was applied to this second isotherm to calculate the specific surface area excluding the consumption of nitrogen corresponding to micropore filling, and it was called specific surface area corrected ($SSA_{corrected}$). Having replicated the analysis three times for one of the samples, we determined the uncertainty of the measurement of $SSA_{corrected}$ to be ca. 5%. The pore size distribution was determined from the desorption stage of the isotherms applying the BJH method. Scanning electron micrographs were obtained with a JEOL 7600F (JEOL, Zaventem, Belgium) operated at 15.0 kV. Samples were placed on a piece of carbon black tape on an aluminum stub. A chromium sputter coating of 10 nm was carried out under vacuum with a Sputter Metal 208 HR (Cressington, Watford, UK). Vapor-phase water adsorption isotherms were acquired at 295 K, using a 3Flex instrument from Micromeritics. Before the adsorption measurements, the samples were degassed overnight under vacuum (6.7 Pa) at 453 K, and distilled water was purified applying freeze–pump–thaw cycles.

3.3. Catalytic Epoxidation of Cyclooctene

The catalytic performance of the synthesized Ti-SiO_2 was evaluated in the epoxidation of cyclooctene (TCI, >90%) with *tert*-butyl hydroperoxide (TBHP, Sigma-Aldrich, Diegem, Belgium, 5.0–6.0 M in decane), as defined in Scheme 1. The initial concentrations of cyclooctene and TBHP were 0.5 and 0.25 M, respectively, whereas the catalyst concentration was 10 g L^{-1}. The reactants were successively added to a 10-mL reactor with 7.8 mL of acetonitrile (VWR Chemicals, France, ≥99.9%) in the presence of 0.1 M dibutyl ether (DBE, TCI, Zwijndrecht, Belgium, >99%) used as internal standard. The reaction temperature was set at 343 K, and the reaction time was 8 h. In addition, 100 µL aliquots were sampled every hour (an aliquot taken at 0.5 h) with a syringe through a septum fitted to the reactor. The experimental setup is shown in Figure S9. The reactant consumption and product formation were followed by gas chromatography (GC) on a SHIMADZU GC-2010 Plus (Shimadzu Benelux, The Netherlands) equipped with a capillary column Shimadzu SH-RTX-5 with a Crossbondx 5%diphenyl/95%dimethyl polysiloxane composition, 30 m, 0.25 mm ID, 0.10 µm film thickness, and a theoretical maximum temperature of 603 K. The temperature program for GC analysis comprised two steps: a first ramp from 333 to 373 K at 7.5 K min^{-1} and a second one from 373 to 513 K at 30 K min^{-1}. The temperatures of the injector and FID detector were 543 and 548 K, respectively. Helium (Praxair, Schoten, Belgium, quality 5.0) was used as carrier gas at a flow rate of 20 mL min^{-1} and 1 µL aliquot was injected into the GC column with a split ratio (SR) of 20.



Scheme 1. Epoxidation reaction of cyclooctene with TBHP as oxidant and Ti-SiO_2 as catalyst.

4. Conclusions

We succeeded in preparing hydrophobic mesoporous Ti-SiO_2 catalysts with effective methyl-functionalization, controlled texture, and improved Ti dispersion through the aerosol-assisted one-pot sol-gel procedure. Tuning the correct methyl precursor (MTES) molar ratio in the catalyst synthesis is crucial to obtain hydrophobized mesoporous Ti-SiO_2 catalysts, but also to prevent the detrimental effect of the addition of this methyl precursor over Ti dispersion and/or the pore network. The increment of the degree of methyl-functionalization of the aerosol-synthesized Ti-SiO_2 catalysts achieved higher degrees of hydrophobicity, while maintaining their mesoporosity and pore size distributions. Beyond the control of the textural properties such as specific surface area and pore size distribution, the aerosol route proved its superiority at obtaining high Ti dispersion, maximizing the

amount of the catalytically active Ti species (FW-Ti), despite the addition of the methyl precursor. This was confirmed by the comparison of the Ti dispersion in methyl-functionalized catalysts synthesized by aerosol-assisted sol-gel with those prepared by conventional sol–gel. Hydrophobic Ti-SiO_2 samples perform much better in the epoxidation of cyclooctene with tert-butyl hydroperoxide than the pristine, more hydrophilic Ti-SiO_2. This tendency was verified after normalization by the specific surface area and by the number of active framework Ti (FW-Ti) species. An excessive degree of methyl-functionalization diminishes the catalyst performance due to lower Ti dispersion. Overall, an appropriate balance of the degree of methyl-functionalization and hydrophobicity of the Ti-SiO_2 mesoporous mixed oxide catalysts allows the improvement of their catalytic performance. All in all, it was demonstrated that the aerosol route is more advantageous than the conventional sol-gel route to prepare functionalized Ti-SiO_2 porous catalysts with improved catalytic properties.

Supplementary Materials: The following are available online at https://www.mdpi.com/2073-4344/11/2/196/s1, Figure S1: Deconvolution analysis using Gaussian functions on TS_Aer-14%Me to assign the chemical shift of the different contributions (i.e., Q^4, Q^3, Q^2 ...), Table S1: Ti-SiO_2 sample with MTES molar ratio of 0.20 calcined at 523, 623, and 723 K, Figure S2: FTIR-ATR spectra of the sample with nominal MTES molar ratio of 0.20 calcined at 623 and 723 K in static air, Figure S3: T-plots constructed based on the N_2 adsorption data for the TS_Aer-x%Me catalysts, Figure S4: SEM images of TS_Aer-0%Me (a) and TS_Aer-9%Me (b), Figure S5: Water vapor adsorption isotherms for TS_Aer-0%Me, TS_Aer -9%Me, and TS_Aer-14%Me at 295 K, Figure S6: Eg calculation from the optical absorption edge in the DRUV spectra for the TS_Aer-x%Me catalysts using the Tauc method, Figure S7: Eg calculation from the optical absorption edge in the DRUV spectra for pristine and methyl-functionalized Ti-SiO_2 catalysts synthesized by conventional sol-gel method using the Tauc method, Table S2: XPS surface elemental quantification, Figure S8: TBHP conversion as a function of reaction time of the TS_Aer-x%Me catalysts, Figure S9: Experimental setup for catalytic tests.

Author Contributions: Conceptualization, C.A., D.P.D. and E.M.G.; Formal analysis, L.E.M.-P., A.V. and P.E.; Funding acquisition, C.A., D.P.D. and E.M.G.; Investigation, L.E.M.-P., V.S., A.V. and I.K.; Methodology, L.E.M.-P., V.S., D.P.D. and E.M.G.; Project administration, C.A., D.P.D. and E.M.G.; Resources, L.E.M.-P., C.A., D.P.D. and E.M.G.; Supervision, C.A., D.P.D. and E.M.G.; Visualization, L.E.M.-P. and E.M.G.; Writing—original draft, L.E.M.-P.; Writing —review and editing, L.E.M.-P., V.S., A.V., I.K., P.E., C.A., D.P.D. and E.M.G. All authors have read and agreed to the published version of the manuscript.

Funding: The authors would like to thank the 'Communauté française de Belgique' for the financial support through the ARC programme (15/20-069). L.E. Manangon-Perugachi acknowledges to SENESCYT (Ecuador) and IFTH (Ecuador) for her PhD grant. V. Smeets is thankful to F.R.S.−F.N.R.S. for his FRIA PhD grant. D.P. Debecker thanks the Francqui foundation for his "Francqui Research Professor" chair. This research used resources of the nuclear magnetic resonance service located at the University of Namur. This service is a member of the "Plateforme Technologique Physico-Chemical Characterization" PC^2. F.R.S.–F.N.R.S. is also acknowledged for (i) the acquisition of the DRUV spectrometer (project CDR J.0156.18, supervisor E.M. Gaigneaux) and (ii) the acquisition of the water vapor sorption equipment used (project EQP U.N030.18, supervisor D.P. Debecker).

Acknowledgments: F. Devred and I. Meza are acknowledged for the technical support in the water vapor adsorption and the DRUV analysis. Luca Fusaro is thanked for his support to the NMR measurements.

Conflicts of Interest: The authors declare no conflict of interest. The funders had no role in the design of the study; in the collection, analyses, or interpretation of data; in the writing of the manuscript, or in the decision to publish the results.

References

1. Fidalgo, A.; Ciriminna, R.; Ilharco, L.M.; Pagliaro, M. Role of the Alkyl−Alkoxide Precursor on the Structure and Catalytic Properties of Hybrid Sol−Gel Catalysts. *Chem. Mater.* **2005**, *17*, 6686–6694. [CrossRef]
2. Swalus, C.; Farin, B.; Gillard, F.; Devillers, M.; Gaigneaux, E.M. Hybrid peroxotungstophosphate organized catalysts highly active and selective in alkene epoxidation. *Catal. Commun.* **2013**, *37*, 80–84. [CrossRef]

3. Cordon, M.J.; Harris, J.W.; Vega-Vila, J.C.; Bates, J.S.; Kaur, S.; Gupta, M.; Witzke, M.E.; Wegener, E.C.; Miller, J.T.; Flaherty, D.W.; et al. Dominant Role of Entropy in Stabilizing Sugar Isomerization Transition States within Hydrophobic Zeolite Pores. *J. Am. Chem. Soc.* **2018**, *140*, 14244–14266. [CrossRef] [PubMed]
4. Vivian, A.; Fusaro, L.; Debecker, D.P.; Aprile, C. Mesoporous Methyl-Functionalized Sn-Silicates Generated by the Aerosol Process for the Sustainable Production of Ethyl Lactate. *ACS Sustain. Chem. Eng.* **2018**, *6*, 14095–14103. [CrossRef]
5. Chen, X.; Qian, P.; Zhang, T.; Xu, Z.; Fang, C.; Xu, X.; Chen, W.; Wu, P.; Shen, Y.; Li, S.; et al. Catalyst surfaces with tunable hydrophilicity and hydrophobicity: Metal-organic frameworks toward controllable catalytic selectivity. *Chem. Commun.* **2018**, *54*, 3936–3939. [CrossRef]
6. Shi, W.; Cao, L.; Zhang, H.; Zhou, X.; An, B.; Lin, Z.; Dai, R.; Li, J.; Wang, C.; Lin, W. Surface Modification of Two-Dimensional Metal–Organic Layers Creates Biomimetic Catalytic Microenvironments for Selective Oxidation. *Angew. Chem. Int. Ed.* **2017**, *56*, 9704–9709. [CrossRef]
7. Li, L.; Yang, Q.; Chen, S.; Hou, X.; Liu, B.; Lu, J.; Jiang, H.-L. Boosting selective oxidation of cyclohexane over a metal–organic framework by hydrophobicity engineering of pore walls. *Chem. Commun.* **2017**, *53*, 10026–10029. [CrossRef]
8. Sun, Q.; He, H.; Gao, W.-Y.; Aguila, B.; Wojtas, L.; Dai, Z.; Li, J.; Chen, Y.-S.; Xiao, F.; Ma, S. Imparting amphiphobicity on single-crystalline porous materials. *Nat. Commun.* **2016**, *7*, 13300. [CrossRef]
9. Khouw, C.; Dartt, C.; Labinger, J.; Davis, M. Studies on the Catalytic-Oxidation of Alkanes and Alkenes by Titanium Silicates. *J. Catal.* **1994**, *149*, 195–205. [CrossRef]
10. Zapata, P.A.; Faria, J.; Ruiz, M.P.; Jentoft, R.E.; Resasco, D.E. Hydrophobic Zeolites for Biofuel Upgrading Reactions at the Liquid–Liquid Interface in Water/Oil Emulsions. *J. Am. Chem. Soc.* **2012**, *134*, 8570–8578. [CrossRef]
11. Zapata, P.A.; Huang, Y.; Gonzalez-Borja, M.A.; Resasco, D.E. Silylated hydrophobic zeolites with enhanced tolerance to hot liquid water. *J. Catal.* **2013**, *308*, 82–97. [CrossRef]
12. Gounder, R. Hydrophobic microporous and mesoporous oxides as Brønsted and Lewis acid catalysts for biomass conversion in liquid water. *Catal. Sci. Technol.* **2014**, *4*, 2877–2886. [CrossRef]
13. Smeets, V.; Ben Mustapha, L.; Schnee, J.; Gaigneaux, E.M.; Debecker, D.P. Mesoporous SiO2-TiO2 epoxidation catalysts: Tuning surface polarity to improve performance in the presence of water. *Mol. Catal.* **2018**, *452*, 123–128. [CrossRef]
14. Taramasso, M.; Perego, G.; Notari, B. Preparation of Porous Crystalline Synthetic Material Comprised of Silicon and Titanium Oxides. U.S. Patent No. 4,410,501, 18 October 1983.
15. Notari, B. Synthesis and Catalytic Properties of Titanium Containing Zeolites. In *Studies in Surface Science and Catalysis*; Grobet, P.J., Mortier, W.J., Vansant, E.F., Schulz-Ekloff, G., Eds.; Elsevier: Amsterdam, The Netherlands, 1988; Volume 37, pp. 413–425.
16. Clerici, M.G. The activity of titanium silicalite-1 (TS-1): Some considerations on its origin. *Kinet. Catal.* **2015**, *56*, 450–455. [CrossRef]
17. Signorile, M.; Crocellà, V.; Damin, A.; Rossi, B.; Lamberti, C.; Bonino, F.; Bordiga, S. Effect of Ti Speciation on Catalytic Performance of TS-1 in the Hydrogen Peroxide to Propylene Oxide Reaction. *J. Phys. Chem. C* **2018**, *122*, 9021–9034. [CrossRef]
18. Bregante, D.T.; Thornburg, N.E.; Notestein, J.M.; Flaherty, D.W. Consequences of Confinement for Alkene Epoxidation with Hydrogen Peroxide on Highly Dispersed Group 4 and 5 Metal Oxide Catalysts. *ACS Catal.* **2018**, *8*, 2995–3010. [CrossRef]
19. Corma, A.; Esteve, P.; Martínez, A. Solvent Effects during the Oxidation of Olefins and Alcohols with Hydrogen Peroxide on Ti-Beta Catalyst: The Influence of the Hydrophilicity-Hydrophobicity of the Zeolite. *J. Catal.* **1996**, *161*, 11–19. [CrossRef]
20. Cordeiro, P.J.; Tilley, T.D. Enhancement of the Catalytic Activity of Titanium-Based Terminal Olefin Epoxidation Catalysts via Surface Modification with Functionalized Protic Molecules. *ACS Catal.* **2011**, *1*, 455–467. [CrossRef]
21. Wu, P.; Tatsumi, T.; Komatsu, T.; Yashima, T. Postsynthesis, Characterization, and Catalytic Properties in Alkene Epoxidation of Hydrothermally Stable Mesoporous Ti-SBA-15. *Chem. Mater.* **2002**, *14*, 1657–1664. [CrossRef]
22. Chiker, F.; Launay, F.; Nogier, J.P.; Bonardet, J.L. Green and selective epoxidation of alkenes catalysed by new TiO2–SiO2SBA mesoporous solids. *Green Chem.* **2003**, *5*, 318–322. [CrossRef]
23. Blasco, T.; Corma, A.; Navarro, M.A.; Pariente, J.P. Synthesis, Characterization, and Catalytic Activity of Ti-MCM-41 Structures. *J. Catal.* **1995**, *156*, 65–74. [CrossRef]
24. Corma, A.; Domine, M.; Gaona, J.A.; Jorda, J.L.; Navarro, M.T.; Rey, F.; Pérez-Pariente, J.; Tsuji, J.; McCulloch, B.; Nemeth, L.T. Strategies to improve the epoxidation activity and selectivity of Ti-MCM-41. *Chem. Commun.* **1998**, 2211–2212. [CrossRef]
25. Fraile, J.M.; García, J.I.; Mayoral, J.A.; Vispe, E.; Brown, D.R.; Naderi, M. Is MCM-41 really advantageous over amorphous silica? The case of grafted titanium epoxidation catalysts. *Chem. Commun.* **2001**, *10*, 1510–1511. [CrossRef]
26. Yu, J.; Feng, Z.; Xu, L.; Li, M.; Xin, Q.; Liu, Z.; Li, C. Ti−MCM-41 Synthesized from Colloidal Silica and Titanium Trichloride: Synthesis, Characterization, and Catalysis. *Chem. Mater.* **2001**, *13*, 994–998. [CrossRef]
27. Fraile, J.M.; García, J.I.; Mayoral, J.A.; Vispe, E. Silica-Supported Titanium Derivatives as Catalysts for the Epoxidation of Alkenes with Hydrogen Peroxide: A New Way to Tuneable Catalytic Activity through Ligand Exchange. *J. Catal.* **2000**, *189*, 40–51. [CrossRef]
28. Fraile, J.M.; García, J.I.; Mayoral, J.A.; Vispe, E. Effect of the Reaction Conditions on the Epoxidation of Alkenes with Hydrogen Peroxide Catalyzed by Silica-Supported Titanium Derivatives. *J. Catal.* **2001**, *204*, 146–156. [CrossRef]
29. Smeets, V.; Boissière, C.; Sanchez, C.; Gaigneaux, E.M.; Peeters, E.; Sels, B.F.; Dusselier, M.; Debecker, D.P. Aerosol Route to TiO2–SiO2Catalysts with Tailored Pore Architecture and High Epoxidation Activity. *Chem. Mater.* **2019**, *31*, 1610–1619. [CrossRef]

30. Beck, C.; Mallat, T.; Baiker, A. On the Limited Selectivity of Silica-Based Epoxidation Catalysts. *Catal. Lett.* **2001**, *75*, 131–136. [CrossRef]
31. Beck, C.; Mallat, T.; Buergi, T.; Baiker, A. Nature of Active Sites in Sol-Gel TiO2–SiO2 Epoxidation Catalysts. *J. Catal.* **2001**, *204*, 428–439. [CrossRef]
32. Hutter, R.; Mallat, T.; Baiker, A. Titania Silica Mixed Oxides. *J. Catal.* **1995**, *153*, 177–189. [CrossRef]
33. Hutter, R.; Mallat, T.; Dutoit, D.; Baiker, A. Titania-silica aerogels with superior catalytic performance in olefin epoxidation compared to large pore Ti-molecular sieves. *Top. Catal.* **1996**, *3*, 421–436. [CrossRef]
34. Dutoit, D.; Schneider, M.; Hutter, R.; Baiker, A. Titania–Silica Mixed Oxides. *J. Catal.* **1996**, *161*, 651–658. [CrossRef]
35. Bordiga, S.; Coluccia, S.; Lamberti, C.; Marchese, L.; Zecchina, A.; Boscherini, F.; Buffa, F.; Genoni, F.; Leofanti, G. XAFS Study of Ti-Silicalite: Structure of Framework Ti(IV) in the Presence and Absence of Reactive Molecules (H2O, NH3) and Comparison with Ultraviolet-Visible and IR Results. *J. Phys. Chem.* **1994**, *98*, 4125–4132. [CrossRef]
36. Oyama, S.T. Chapter 1—Rates, Kinetics, and Mechanisms of Epoxidation: Homogeneous, Heterogeneous, and Biological Routes. In *Mechanisms in Homogeneous and Heterogeneous Epoxidation Catalysis*; Elsevier: Amsterdam, The Netherlands, 2008; pp. 3–99. [CrossRef]
37. Clerici, M.G.; Kholdeeva, O.A. *Liquid Phase Oxidation via Heterogeneous Catalysis: Organic Synthesis and Industrial Applications*; John Wiley & Sons: Hoboken, NJ, USA, 2013.
38. Gao, X.; Wachs, I.E. Titania–silica as catalysts: Molecular structural characteristics and physico-chemical properties. *Catal. Today* **1999**, *51*, 233–254. [CrossRef]
39. Thomas, J.M.; Sankar, G.; Klunduk, M.C.; Attfield, M.P.; Maschmeyer, T.; Johnson, B.F.G.; Bell, R.G. The Identity in Atomic Structure and Performance of Active Sites in Heterogeneous and Homogeneous, Titanium−Silica Epoxidation Catalysts. *J. Phys. Chem. B* **1999**, *103*, 8809–8813. [CrossRef]
40. Bregante, D.T.; Flaherty, D.W. Periodic Trends in Olefin Epoxidation over Group IV and V Framework-Substituted Zeolite Catalysts: A Kinetic and Spectroscopic Study. *J. Am. Chem. Soc.* **2017**, *139*, 6888–6898. [CrossRef]
41. Liang, X.; Mi, Z.; Wu, Y.; Wang, L.; Xing, E. Kinetics of epoxidation of propylene over TS-1 in isopropanol. *React. Kinet. Catal. Lett.* **2003**, *80*, 207–215. [CrossRef]
42. Ruddy, D.A.; Tilley, T.D. Kinetics and Mechanism of Olefin Epoxidation with Aqueous H2O2and a Highly Selective Surface-Modified TaSBA15 Heterogeneous Catalyst. *J. Am. Chem. Soc.* **2008**, *130*, 11088–11096. [CrossRef]
43. Thangaraj, A.; Sivasanker, S. An improved method for TS-1 synthesis: 29Si NMR studies. *J. Chem. Soc. Chem. Commun.* **1992**, *10*, 123–124. [CrossRef]
44. Notestein, J.M.; Iglesia, E.; Katz, A. Grafted Metallocalixarenes as Single-Site Surface Organometallic Catalysts. *J. Am. Chem. Soc.* **2004**, *126*, 16478–16486. [CrossRef]
45. Fan, W.; Duan, R.-G.; Yokoi, T.; Wu, P.; Kubota, Y.; Tatsumi, T. Synthesis, Crystallization Mechanism, and Catalytic Properties of Titanium-Rich TS-1 Free of Extraframework Titanium Species. *J. Am. Chem. Soc.* **2008**, *130*, 10150–10164. [CrossRef] [PubMed]
46. Fan, W.; Wu, P.; Tatsumi, T. Unique solvent effect of microporous crystalline titanosilicates in the oxidation of 1-hexene and cyclohexene. *J. Catal.* **2008**, *256*, 62–73. [CrossRef]
47. Fraile, J.M.; García, J.I.; Mayoral, J.A.; Vispe, E. Optimization of cyclohexene epoxidation with dilute hydrogen peroxide and silica-supported titanium catalysts. *Appl. Catal. A Gen.* **2003**, *245*, 363–376. [CrossRef]
48. Langhendries, G.; De Vos, D.E.; Baron, G.V.; Jacobs, P.A. Quantitative Sorption Experiments on Ti-Zeolites and Relation with α-Olefin Oxidation by H2O2. *J. Catal.* **1999**, *187*, 453–463. [CrossRef]
49. Blasco, T.; Camblor, M.A.; Corma, A.; Esteve, P.; Guil, J.M.; Martínez, A.; Perdigón-Melón, A.J.A.; Valencia, S. Direct Synthesis and Characterization of Hydrophobic Aluminum-Free Ti−Beta Zeolite. *J. Phys. Chem. B* **1998**, *102*, 75–88. [CrossRef]
50. Blasco, T.; Camblor, M.A.; Corma, A.; Esteve, P.; Martínez, A.; Prieto, C.; Valencia, S. Unseeded synthesis of Al-free Ti-β zeolite in fluoride medium: A hydrophobic selective oxidation catalyst. *Chem. Commun.* **1996**, *10*, 2367–2368. [CrossRef]
51. Tatsumi, T.; Koyano, K.A.; Igarashi, N. Remarkable activity enhancement by trimethylsilylation in oxidation of alkenes and alkanes with H2O2 catalyzed by titanium-containing mesoporous molecular sieves. *Chem. Commun.* **1998**, 325–326. [CrossRef]
52. Brutchey, R.L.; Ruddy, D.A.; Andersen, L.K.; Tilley, T.D. Influence of Surface Modification of Ti−SBA15 Catalysts on the Epoxidation Mechanism for Cyclohexene with Aqueous Hydrogen Peroxide. *Langmuir* **2005**, *21*, 9576–9583. [CrossRef]
53. Li, S.; Zhou, H.; Xiao, L.; Fan, J.; Zheng, X. Fabrication of Super-Hydrophobic Titanosilicate Sub-micro Sphere with Enhanced Epoxidation Catalytic Activity. *Catal. Lett.* **2019**, *149*, 1396–1402. [CrossRef]
54. Guo, Y.; Hwang, S.-J.; Katz, A. Hydrothermally robust Ti/SiO2 epoxidation catalysts via surface modification with oligomeric PMHS. *Mol. Catal.* **2019**, *477*, 110509. [CrossRef]
55. D'Amore, M.B.; Schwarz, S. Trimethylsilylation of ordered and disordered titanosilicates: Improvements in epoxidation with aqueous H2O2 from micro- to meso-pores and beyond†. *Chem. Commun.* **1999**, 121–122. [CrossRef]
56. Figueras, F.; Kochkar, H. Effects of hydrophobicity on the epoxidation of cyclohexene by tert-butyl hydroperoxide on TiO2–SiO2 mixed oxides. *Catal. Lett.* **1999**, *59*, 79–81. [CrossRef]
57. Kochkar, H.; Figueras, F. Synthesis of Hydrophobic TiO2–SiO2Mixed Oxides for the Epoxidation of Cyclohexene. *J. Catal.* **1997**, *171*, 420–430. [CrossRef]

58. Lin, K.; Pescarmona, P.P.; Houthoofd, K.; Liang, D.; Van Tendeloo, G.; Jacobs, P.A. Direct room-temperature synthesis of methyl-functionalized Ti-MCM-41 nanoparticles and their catalytic performance in epoxidation. *J. Catal.* **2009**, *263*, 75–82. [CrossRef]
59. Klein, S.; Maier, W.F. Microporous Mixed Oxides—Catalysts with Tunable Surface Polarity. *Angew. Chem. Int. Ed.* **1996**, *35*, 2230–2233. [CrossRef]
60. Müller, C.; Deck, R.; Mallat, T.; Baiker, A. Hydrophobic titania–silica aerogels: Epoxidation of cyclic compounds. *Top. Catal.* **2000**, *11*, 369–378. [CrossRef]
61. Müller, C.; Maciejewski, M.; Mallat, T.; Baiker, A. Organically Modified Titania–Silica Aerogels for the Epoxidation of Olefins and Allylic Alcohols. *J. Catal.* **1999**, *184*, 280–293. [CrossRef]
62. Perugachi, L.E.M.; Vivian, A.; Eloy, P.; Debecker, D.P.; Aprile, C.; Gaigneaux, E.M. Hydrophobic titania-silica mixed oxides for the catalytic epoxidation of cyclooctene. *Catal. Today* **2019**. [CrossRef]
63. Debecker, D.P.; Le Bras, S.; Boissière, C.; Chaumonnot, A.; Sanchez, C. Aerosol processing: A wind of innovation in the field of advanced heterogeneous catalysts. *Chem. Soc. Rev.* **2018**, *47*, 4112–4155. [CrossRef]
64. Godard, N.; Vivian, A.; Fusaro, L.; Cannavicci, L.; Aprile, C.; Debecker, D.P. High-Yield Synthesis of Ethyl Lactate with Mesoporous Tin Silicate Catalysts Prepared by an Aerosol-Assisted Sol-Gel Process. *ChemCatChem* **2017**, *9*, 2211–2218. [CrossRef]
65. Kim, A.; Sanchez, C.; Haye, B.; Boissière, C.; Sassoye, C.; Debecker, D.P. Mesoporous TiO2 Support Materials for Ru-Based CO2 Methanation Catalysts. *ACS Appl. Nano Mater.* **2019**, *2*, 3220–3230. [CrossRef]
66. Wang, C.Y.; Bai, H. Aerosol processing of mesoporous silica supported bimetallic catalysts for low temperature acetone oxidation. *Catal. Today* **2011**, *174*, 70–78. [CrossRef]
67. Pega, S.; Boissière, C.; Grosso, D.; Azaïs, T.; Chaumonnot, A.; Sanchez, C. Direct Aerosol Synthesis of Large-Pore Amorphous Mesostructured Aluminosilicates with Superior Acid-Catalytic Properties. *Angew. Chem. Int. Ed.* **2009**, *48*, 2784–2787. [CrossRef] [PubMed]
68. Maksasithorn, S.; Praserthdam, P.; Suriye, K.; Debecker, D.P. Preparation of super-microporous WO3–SiO2 olefin metathesis catalysts by the aerosol-assisted sol-gel process. *Microporous Mesoporous Mater.* **2015**, *213*, 125–133. [CrossRef]
69. Oveisi, H.; Suzuki, N.; Beitollahi, A.; Yamauchi, Y. Aerosol-assisted fabrication of mesoporous titania spheres with crystallized anatase structures and investigation of their photocatalitic properties. *J. Sol. Gel Sci. Technol.* **2010**, *56*, 212–218. [CrossRef]
70. Liu, Z.; Hua, Y.; Wang, J.; Dong, X.; Tian, Q.; Han, Y. Recent progress in the direct synthesis of hierarchical zeolites: Synthetic strategies and characterization methods. *Mater. Chem. Front.* **2017**, *1*, 2195–2212. [CrossRef]
71. Ghosh, M.; Lohrasbi, M.; Chuang, S.S.C.; Jana, S.C. Mesoporous Titanium Dioxide Nanofibers with a Significantly Enhanced Photocatalytic Activity. *ChemCatChem* **2016**, *8*, 2525–2535. [CrossRef]
72. Sing, K.S.W. Reporting physisorption data for gas/solid systems with special reference to the determination of surface area and porosity (Recommendations 1984). *Pure Appl. Chem.* **1985**, *57*, 603–619. [CrossRef]
73. Bregante, D.T.; Johnson, A.M.; Patel, A.Y.; Ayla, E.Z.; Cordon, M.J.; Bukowski, B.C.; Greeley, J.P.; Gounder, R.; Flaherty, D.W. Cooperative Effects between Hydrophilic Pores and Solvents: Catalytic Consequences of Hydrogen Bonding on Alkene Epoxidation in Zeolites. *J. Am. Chem. Soc.* **2019**, *141*, 7302–7319. [CrossRef]
74. Olson, D.; Haag, W.; Borghard, W. Use of water as a probe of zeolitic properties: Interaction of water with HZSM-5. *Microporous Mesoporous Mater.* **2000**, *35-36*, 435–446. [CrossRef]
75. Ng, E.-P.; Mintova, S. Nanoporous materials with enhanced hydrophilicity and high water sorption capacity. *Microporous Mesoporous Mater.* **2008**, *114*, 1–26. [CrossRef]
76. Zecchina, A.; Spoto, G.; Bordiga, S.; Ferrero, A.; Petrini, G.; Leofanti, G.; Padovan, M. Framework and Extraframework Ti in Titanium-Silicalite: Investigation by Means of Physical Methods. In *Studies in Surface Science and Catalysis*; Elsevier BV: Amsterdam, The Netherlands, 1991; Volume 69, pp. 251–258.
77. Klein, S.; Weckhuysen, B.; Martens, J.; Maier, W.; Jacobs, P.A. Homogeneity of Titania-Silica Mixed Oxides: On UV-DRS Studies as a Function of Titania Content. *J. Catal.* **1996**, *163*, 489–491. [CrossRef]
78. Ikeue, K.; Ikeda, S.; Watanabe, A.; Ohtani, B. Elucidation of the local structure of active titanium(iv) sites on silica-based phase-boundary catalysts for alkene epoxidation with aqueous hydrogen peroxide. *Phys. Chem. Chem. Phys.* **2004**, *6*, 2523–2528. [CrossRef]
79. On, D.T.; Bonneviot, L.; Le Noc, L. Electron transfer bands of titanium sites in dehydrated silicalites and in TiO2–SiO2gel. *Chem. Commun.* **1996**, *10*, 299–300. [CrossRef]
80. De Clercq, R.; Dusselier, M.; Poleunis, C.; Debecker, D.P.; Giebeler, L.; Oswald, S.; Makshina, E.; Sels, B.F. Titania-Silica Catalysts for Lactide Production from Renewable Alkyl Lactates: Structure–Activity Relations. *ACS Catal.* **2018**, *8*, 8130–8139. [CrossRef]
81. Viezbicke, B.D.; Patel, S.; Davis, B.E.; Birnie, D.P. Evaluation of the Tauc method for optical absorption edge determination: ZnO thin films as a model system. *Phys. Status Solidi (b)* **2015**, *252*, 1700–1710. [CrossRef]
82. Wagner, C.; Riggs, W.; Davis, L.; Moulder, J.; Muilenberg, G. *Handbook of X-Ray Photoelectron Spectroscopy*; Muilenberg, G., Ed.; Perkin-Elmer Corporation, Physical Electronics Division: Eden Prairie, MN, USA, 1979.
83. Stakheev, A.Y.; Shpiro, E.S.; Apijok, J. XPS and XAES study of titania-silica mixed oxide system. *J. Phys. Chem.* **1993**, *97*, 5668–5672. [CrossRef]
84. Tyablikov, I.A.; Rodionova, L.I.; Sobolev, P.D.; Ivanova, I.I. Formation of active sites in titanium-containing zeolites with MFI structure in propylene epoxidation with hydrogen peroxide. *Pet. Chem.* **2016**, *56*, 267–274. [CrossRef]

85. Yamashita, H.; Kawasaki, S.; Ichihashi, Y.; Harada, M.; Takeuchi, A.M.; Anpo, M.; Stewart, G.; Fox, M.A.; Louis, C.; Che, M. Characterization of Titanium–Silicon Binary Oxide Catalysts Prepared by the Sol-Gel Method and Their Photocatalytic Reactivity for the Liquid-Phase Oxidation of 1-Octanol. *J. Phys. Chem. B* **1998**, *102*, 5870–5875. [CrossRef]
86. Langerame, F.; Salvi, A.M.; Silletti, M.; Moretti, G. XPS characterization of a synthetic Ti-containing MFI zeolite framework: The titanosilicalites, TS-1. *Surf. Interface Anal.* **2008**, *40*, 695–699. [CrossRef]
87. Vetter, S.; Schulz-Ekloff, G.; Kulawik, K.; Jaeger, N.I. On the para/ortho product ratio of phenol and anisole hydroxylation over titanium silicalite-1. *Chem. Eng. Technol.* **1994**, *17*, 348–353. [CrossRef]
88. Hasegawa, Y.; Ayame, A. Investigation of oxidation states of titanium in titanium silicalite-1 by X-ray photoelectron spectroscopy. *Catal. Today* **2001**, *71*, 177–187. [CrossRef]
89. Erdem, B.; Hunsicker, R.A.; Simmons, G.W.; Sudol, E.D.; Dimonie, V.L.; El-Aasser, M.S. XPS and FTIR Surface Characterization of TiO2Particles Used in Polymer Encapsulation. *Langmuir* **2001**, *17*, 2664–2669. [CrossRef]